The spine neck filters membrane potentials

Roberto Araya, Jiang Jiang*, Kenneth B. Eisenthal†, and Rafael Yuste†

Howard Hughes Medical Institute and Departments of Biological Sciences and Chemistry, Columbia University, New York, NY 10027

Contributed by Kenneth B. Eisenthal, October 5, 2006 (sent for review August 21, 2006)

Dendritic spines receive most synaptic inputs in the forebrain. Their morphology, with a spine head isolated from the dendrite by a slender neck, indicates a potential role in isolating inputs. Indeed, biochemical compartmentalization occurs at spine heads because of the diffusional bottleneck created by the spine neck. Here we investigate whether the spine neck also isolates inputs electrically. Using two-photon uncaging of glutamate on spine heads from mouse layer-5 neocortical pyramidal cells, we find that the amplitude of uncaging potentials at the soma is inversely proportional to neck length. This effect is strong and independent of the position of the spine in the dendritic tree and size of the spine head. Moreover, spines with long necks are electrically silent at the soma, although their heads are activated by the uncaging event, as determined with calcium imaging. Finally, second harmonic measurements of membrane potential reveal an attenuation of somatic voltages into the spine head, an attenuation directly proportional to neck length. We conclude that the spine neck plays an electrical role in the transmission of membrane potentials, isolating synapses electrically.

second harmonic | electrical isolation | uncaging | cortex | glutamate

The dendritic spine is a ubiquitous feature in the nervous system, whose function is still poorly understood and heavily investigated (1). Spines are recipients of excitatory inputs in many neurons, including pyramidal cells (2), but excitatory inputs in nonspiny neurons contact dendritic shafts. Therefore, rather than just serving as recipients of inputs, spines likely perform a specific function with those inputs. Indeed, spines are calcium compartments and can therefore restrict local biochemical reactions to single inputs (3, 4). Nevertheless, nonspiny neurons can also perform similar calcium compartmentalization (5, 6), so it is conceivable that spines could implement an additional function.

Theoretical work, spanning several decades, has proposed that spines could play an important role in altering synaptic potentials (7–12) (for a recent review, see ref. 13). Because of the resistance of the spine neck, spines could electrically isolate inputs and thus prevent input resistance variations in the dendrite during synaptic transmission (8). Thus, excitatory synaptic potentials could be filtered when they reach the dendrite (8–10, 12).

The resistance of the spine neck, a crucial variable in ascertaining the electrical function of the spine, has never been measured. Estimates made from passive cable models (14) or diffusional coupling (15) would make its value too low to significantly filter synaptic potentials. At the same time, recent diffusional estimates indicate that neck resistances could be higher (16). Indeed, in our recent work examining input integration, we found that potentials onto spines sum linearly, whereas depolarizations on dendritic shafts shunt each other (R.A., K.B.E., and R.Y., unpublished work). Thus, our data would imply that spines isolate inputs electrically.

We have tested whether the spine neck plays an electrical role by combining whole-cell recordings with two-photon glutamate uncaging of glutamate onto spines from layer-5 pyramidal neurons in brain slices from mouse visual cortex, and we have analyzed uncaging potentials from spines with different neck lengths. We find that the spine neck length is inversely correlated with the amplitude of the uncaging potential, as measured in the soma. We also encounter spines with long necks that are electrically silent at the soma, although with calcium imaging we demonstrate that those long spines can be activated normally. Finally, using second harmonic generation (SHG) imaging of membrane potential of spines (17), we demonstrate that voltage pulses that originate at the soma are attenuated at the spine head and that this attenuation is also proportional to the length of the spine neck. Thus, voltage pulses propagating to the spine or from the spine are attenuated in proportion to the length of the spine neck. Our data indicate that the spine neck filters membrane potentials and that spines can isolate inputs electrically.

Results

Generation of Spine Uncaging Potentials. We were interested in testing the role of the spine neck in the transmission of electrical signals from the spine head to the dendritic shaft. For this purpose, we used two-photon uncaging of glutamate (18) to activate spines with different neck lengths. Experiments were performed in brain slices from P14-20 mouse primary visual cortex. Layer-5 pyramidal neurons were patched with whole-cell electrodes, filled with Alexa 488, and imaged with a custom-built two-photon microscope (Fig. 1*A*). We studied the responses of spines in basal dendrites (Fig. 1*A Inset*), mostly at distances of $\approx$20–80 μm from the soma. This is a population of spines that we have previously characterized morphologically and that constitutes a large proportion of the spines in this class of neurons (19, 20).

For these experiments, we recorded the somatic depolarization after uncaging glutamate at the head of the spine, a signal that we termed "uncaging potential." The glutamate uncaging protocol chosen for this study was the same for all spines, positioning the uncaging laser at the edge of the spine, within $\approx$0.2 μm of its membrane, and using a 4-ms laser uncaging pulse with 2.5 mM extracellular concentration of 4-methoxy-7-nitroindoline-caged L-gluamate (21). We characterized the spatial resolution of our uncaging method by moving the laser perpendicular to the dendrite from 0.2 to 2.2 μm away from the spine head edge (Fig. 1*B*). Uncaging 0.2 μm away from the spine head generated a voltage deflection at the soma (0.86 $\pm$ 0.08 mV, $n = 10$; Fig. 1*B*, position 1) that was practically abolished by parking the laser 0.8 μm away (0.1 $\pm$ 0.07 mV, $n = 10$; Fig. 1*B*, position 2). Moving the laser $>$1.5 μm away from the spine head did not generate any appreciable voltage deflection at the soma (Fig. 1*B*). In addition, uncaging next to the spine head in the absence of 4-methoxy-7-nitroindoline-caged L-glutamate with similar power levels did not produce any voltage deflection at the soma (data not shown). Thus, our experimental technique had appropriate spatial resolution to generate localized depolarizations with single spine resolution.

Author contributions: K.B.E. and R.Y. designed research; R.A. and J.J. performed research; R.A., J.J., K.B.E., and R.Y. analyzed data; and K.B.E. and R.Y. wrote the paper.

The authors declare no conflict of interest.

Abbreviations: SHG, second harmonic generation; EPSP, excitatory postsynaptic potential.

*Present address: Institute of Bioengineering and Nanotechnology, 31 Biopolis Way, The Nanos no. 04-01, Republic of Singapore 138669.

†To whom correspondence may be addressed. E-mail: rmy5@columbia.edu or kbe1@columbia.edu.

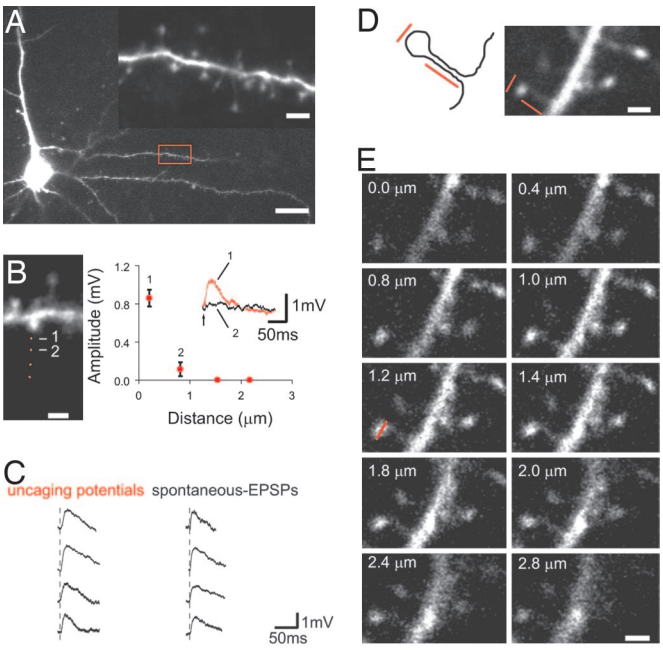

Fig. 1. Spine glutamate uncaging and morphological reconstructions. (*A*) Layer-5 pyramidal cell filled with Alexa Fluor 488. (Scale bar: 20 μm.) (*Inset*) Representative basal dendrite selected for uncaging. (Scale bar: 3 μm.) (*B*) Spatial resolution of uncaging. Red dots indicate the site of uncaging when laser beam was parked at different distances away from the head of the spine (≈0.2–2 μm). (Scale bar: 1 μm.) Graph shows effect of distance on uncaging potentials. Peak amplitude drops to zero if laser is 1.5 μm away from the spine head. *Inset* shows the average of 10 uncaging EPSPs at position 0.2 μm (red trace, position 1) and 0.8 μm (black trace, position 2) away from the spine head. (*C*) Comparison of spontaneous EPSPs and EPSPs after two-photon uncaging of glutamate (uncaging potentials). Dashed line indicates onset of glutamate uncaging or spontaneous events. (*D*) Neck length was measured from the base of the spine head toward the edge of the dendrite (orthogonal red line), and the head diameter was estimated by measuring the longest possible axis at any of the *z*-stacks of images as shown in *E*. (Scale bar: 1 μm.)

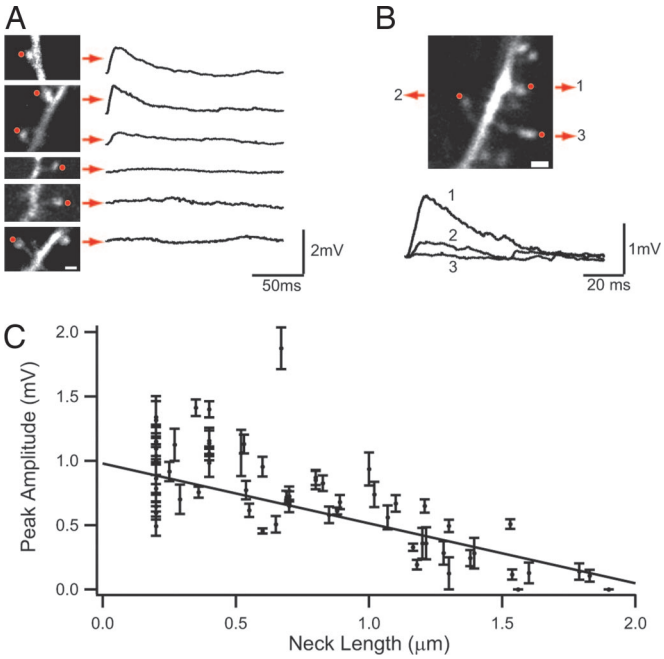

Fig. 2. Effect of spine neck length on spine potentials. (*A*) Examples of uncaging potentials in spines with short and long necks. Red dots indicate the site of uncaging and traces corresponded to averages of ≈10 uncaging potentials for each spine. (*B*) Three neighboring spines (1, 2, and 3) with different neck lengths. Note the large difference in their uncaging potentials at the soma. (*C*) Plot of the uncaging potentials (peak amplitude) vs. neck length. Line is linear regression of the data, with a weighted fit including the standard error of each data point.

For all spines, uncaging potentials ranged from 0 to 2 mV (0.72 ± 0.05 mV, $n = 58$ spines) and were somewhat smaller on average than spontaneously occurring excitatory postsynaptic potentials (EPSPs) (Fig. 1*C*; 0.86 ± 0.07 mV for spontaneous EPSPs, $n = 61$, $P < 0.01$). The kinetics of uncaging potentials ranged from ≈0.002 to 0.3 mV/ms in 10/90 rate of rise and from ≈40 to 300 ms in duration, slower than spontaneous EPSPs (0.07 ± 0.008 mV/ms in 10/90 rate of rise, $n = 56$ spines for uncaging potentials vs. 0.25 ± 0.03 mV/ms, $n = 61$ for spontaneous potentials, $P < 0.01$, *t* test; 124 ± 9-ms duration, $n = 56$ spines for uncaging potentials vs. 50.4 ± 4 ms, $n = 61$ for spontaneous potentials, $P < 0.001$). However, the kinetics of the larger uncaging potentials (≥1.1 mV; 1.32 ± 0.08 mV average amplitude; 0.38 μm average neck length; $n = 9$ spines) were similar in 10/90 rate of rise to spontaneous EPSPs although they still had longer durations (0.167 ± 0.039 mV/ms, $n = 9$ spines, $P = 0.068$; 111.73 ± 12.15-ms duration, $n = 9$ spines, $P < 0.001$).

We captured the morphology of each characterized spine in three dimensions with a stack of two-photon images (Fig. 1*D*). We used these z-stacks to measure spine neck lengths and spine head diameters (Fig. 1 *D* and *E*). Spine necks ranged from 0.2 to ≈2 μm, and head diameters ranged from 0.5 to 1.2 μm (average = 0.77 ± 0.06 μm in length and 0.77 ± 0.02 μm in diameter, $n = 58$ spines). These values are comparable to those measured in our light-level morphological studies of this same population of neurons (19) and our recent ultrastructural reconstruction of spines from mouse primary visual cortex (J. I. Arellano, A. Espinosa, A. Fairen, R.Y., and J. DeFelipe, unpublished work).

Effect of Spine Neck Length on Uncaging Potentials. We inquired whether there was a correlation between the spine neck length and the amplitude of the uncaging potential, measured at the soma. Indeed, a strong negative correlation was present, whereby uncaging potentials onto spines with shorter necks were larger than uncaging potentials of spines with longer necks (Fig. 2). A linear fit to the function gave an R of −0.75 and a slope of −0.46 ± 0.01 mV/μm (Fig. 2*C*). This result was significantly different when compared with the null hypothesis of a zero slope ($P < 0.001$, ANOVA). Using the top and bottom quartiles of the distributions for comparison, spines with the longest neck had an average amplitude of 0.25 ± 0.04 mV, whereas spines with the shortest neck had an average amplitude of 0.95 ± 0.06 mV ($P < 0.001$, *t* test).

We performed a similar analysis on the kinetics of the uncaging events and found an inverse correlation between the 10/90 rate of rise of the uncaging potentials with the neck length (Fig. 3*A*; $R = 0.5$, slope = −0.068 ± 0.015 mVms/μm, $P < 0.001$, ANOVA). In addition, the linear fit to the duration of the events vs. the neck length showed a weak negative correlation (Fig. 3*B*; $R = 0.3$, slope = −44.42 ± 18.2 ms/μm, $P = 0.015$, ANOVA).

The Effect of the Spine Neck Is Independent of Spine Position and Head Diameter. We wondered whether the dependency between the spine neck and amplitude of uncaging potentials, as measured at the soma, was influenced by the electrical filtering in the dendritic shaft. To examine this, we analyzed the data with respect to the distance from the soma of the activated spines. Our rationale was that if dendritic filtering were significant, it would scale with the length of the dendrite and thus reveal itself as a

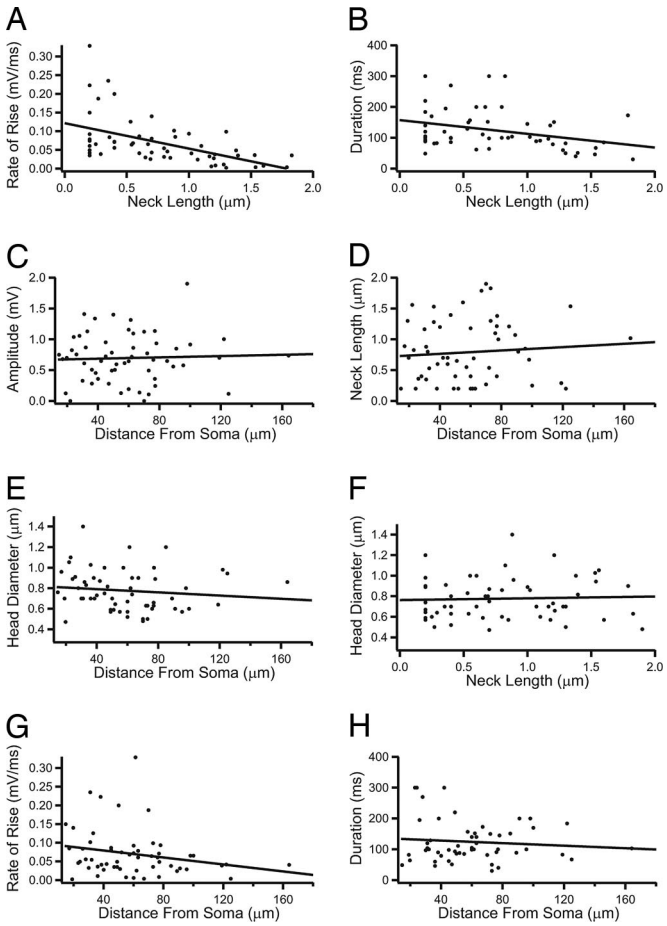

Fig. 3. Correlations between morphological variables and uncaging potentials. (*A* and *B*) Correlation between the 10/90 rate of rise (*A*) and duration (*B*) of the uncaging potentials and neck length. (*C–F*) Correlations between peak amplitude (*C*), neck lengths (*D*), spine head diameter (*E* and *F*), 10/90 rate of rise (*G*), and duration of uncaging potentials (*H*) with distance of the spines from soma and between the spine head diameter and the spine neck length (*F*). Lines are linear fit (for values, see *Results*).

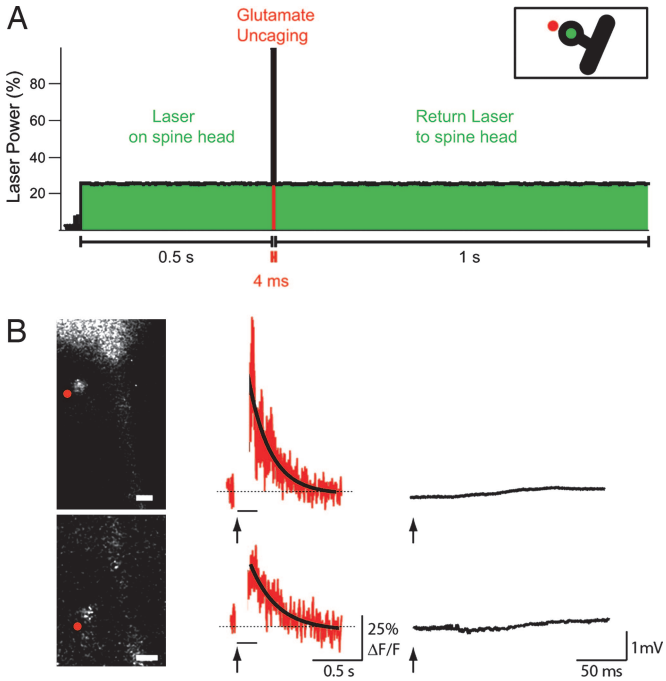

Fig. 4. Long spines are activated by glutamate uncaging. (*A*) Protocol for the measurement of the intracellular free calcium at the head of the spine. (*B*) Two examples of long neck spines from a layer-5 pyramidal cell filled with Calcium Green-1. Red trace corresponded to the average measurements of the intracellular free calcium in the head of the spine indicated in response to the uncaging pulse. Black traces correspond to the average uncaging potential of the corresponding spine. Red dots indicate the site of uncaging. (Scale bar: 1 μm.)

systematic trend with respect to the distance to the soma of the activated spine. In this analysis, however, we did not observe a relation between the amplitude of the uncaging potential and the distance of the spine to the soma (Fig. 3*C*; $R = 0.04$, slope = 0.0005 ± 0.0017 mV/μm, $P = 0.75$, ANOVA). In fact, our sample included spines located close (≈15 μm) to the soma, where the filtering would be minimized, and, even in these spines, a strong modulation of uncaging potential with neck length was present. Specifically, in spines at ≤40 μm from the soma, there was still a strong inverse correlation between the amplitude of the uncaging potentials and the neck length ($R = 0.8$, slope = -0.95 ± 0.15 mV/μm, $P < 0.001$, ANOVA). Moreover, the spine neck length was not correlated with the distance from the soma (Fig. 3*D*; $R = 0.08$, slope = 0.001 ± 0.002, $P = 0.6$, ANOVA), ruling out a systematic regulation of the spine neck lengths along the basal dendrite of layer-5 pyramidal cells.

We also wondered whether the spine head diameter was correlated with the amplitude of the uncaging potential, an effect described previously in CA1 pyramidal neurons (18). Spine head diameters were estimated from z-stacks as described above (Fig. 1 *D* and *E*). In our sample of neocortical spines, however, we did not detect a correlation between the spine head diameter and the amplitude ($R = 0.1$, slope = 0.2 ± 0.2 mV/μm, $P = 0.4$, ANOVA), 10/90 rate of rise ($R = 0.1$, slope = 0.04 ± 0.04, $P = 0.2$, ANOVA), or duration of the uncaging potential ($R = 0.19$, slope = 64.03 ± 45.9 ms/μm, $P = 0.19$, ANOVA). No significant correlation was present even for spines with similar neck lengths (for spines with necks lengths <0.4 μm, $R = 0.35$, $P = 0.16$, $n = 17$) Moreover, the diameter of the spine head was uncorrelated with the spine neck length (Fig. 3*F*; $R = 0.04$, slope = 0.017 ± 0.05, $P = 0.9$, ANOVA), in agreement with our past morphological studies (19). Also, the spine head diameter was not regulated as a function of the distance from the soma (Fig. 3*E*; $R = 0.1$, slope = -0.0007 ± 0.0008, $P = 0.23$, ANOVA). Finally, there was a very weak correlation between the 10/90 rate of rise and the distance from soma (Fig. 3*G*; $R = 0.22$, slope = -0.00046 ± 0.00027 mVms/μm, $P = 0.1$, ANOVA) and no correlation between the duration of the uncaging potentials and the distance from soma (Fig. 3*H*; R = 0.1, slope = -0.2 ± 0.3 ms/μm, $P = 0.46$, ANOVA).

We concluded that the spine neck length modulates the strength of the uncaging potential. This effect is not explained by the position of the spine or the diameter of the spine head, as though the spine neck length were independently regulated at each spine.

Long-Necked Spines Are Activated by Glutamate Uncaging. Our data thus revealed a population of spines that had long necks but whose stimulation with glutamate uncaging failed to generate any appreciable depolarization at the soma (see Fig. 2). We wondered whether these long spines were indeed activated by the glutamate uncaging. To test this hypothesis, we filled neurons with the calcium indicator Calcium Green-1 and performed two-photon fluorescence measurements of changes in intracellular free calcium at the head of the spine (3) (Fig. 4). These

results indicated that long spines had similar calcium responses to glutamate uncaging as shorter spines (Fig. 4*B*). Specifically, uncaging pulses generated calcium transients in long spines (>1.5 μm neck length) that were 42 ± 10% in amplitude (n = 5) with decay times (τ) of 0.2 ± 0.01 s (n = 3) and τ >1 s (n = 2). Similar calcium transients were observed in short spines (<1 μm neck length; 46 ± 7.6% in amplitude, n = 5 and decay times with τ = 0.14 s; n = 2 and τ >1 s; n = 3 spines). Overall, there was no correlation between neck lengths and amplitude of calcium transients at the spine heads (R = 0.06, P = 0.86, n = 10). Among the spines longer than 1.5 μm, there was also no correlation between neck length and amplitude of calcium transient (R = 0.34, P = 0.56, n = 5). Simultaneous with these measurements, recordings of membrane potential at the soma in longer spines revealed no discernible voltage depolarization, even in spines close to the soma (Fig. 4*B*; five of five experiments).

Given these results, we wondered whether spines with long necks were different in head diameter to shorter neck spines. Using the top and bottom quartiles of the distributions for comparison, we found that spines with the longest necks had an average head diameter of 0.79 ± 0.05 μm, whereas the spines with the shortest necks an average head diameter of 0.75 ± 0.04 μm (P = 0.5, t test). Thus, the longest spines had head diameters within the norm of the other spines.

Our data thus indicate that long-necked spines were indeed being activated and, because they respond to caged glutamate, likely have glutamate receptors. At the same time, their long necks must severely attenuate their potentials to the point that they are electrically silent at the soma.

Filtering of Somatic Potentials by Spine Neck. After establishing that spine potentials were filtered when they propagate through the spine neck toward the soma, we wondered whether the spine neck was also filtering somatic potentials as they propagate toward the spine head. For this purpose, we used SHG imaging of membrane potential at the spine. SHG is a nonlinear optical phenomenon that is interface selective (22). Its linear dependence on voltage, as demonstrated by several groups (23–26), makes it ideally suited to image membrane potential. Indeed, using this optical technique, we recently performed the first experimental measurements of voltage at spines (17), observing a linear dependency of SHG signals with membrane potential and a nondecremental action potential invasion into dendritic spines.

We now used SHG to examine how somatic voltage clamp pulses propagate to the head of the spine and whether the spine neck influenced this propagation. For these experiments, we filled the neurons with the SHG chromophore FM 4-64 (Fig. 5*A*) and, while voltage-clamping the neuron, measured the SHG response at the head of the spine and adjacent dendritic shaft (Fig. 5*B*; voltage clamp pulses 30–50 mV in amplitude and 5–20 s in duration). Our results, obtained from 22 spines of 9 neurons, showed a voltage modulation of the SHG signal of spine heads in response to somatic voltages, as reported in ref. 17. However, the magnitude of the voltage transmission from soma to spine head depended on the spine neck length (Fig. 5*C*). The SHG response, which is linearly proportional to membrane voltage, was inversely proportional to the spine neck length. A linear fit to the data had an R value of −0.57 and a slope of −0.37 ± 0.06 (P = 0.007 vs. zero slope, ANOVA). This slope (rate of voltage attenuation) was somewhat smaller than that of the uncaging potential dependency on spine neck (Fig. 2*C*).

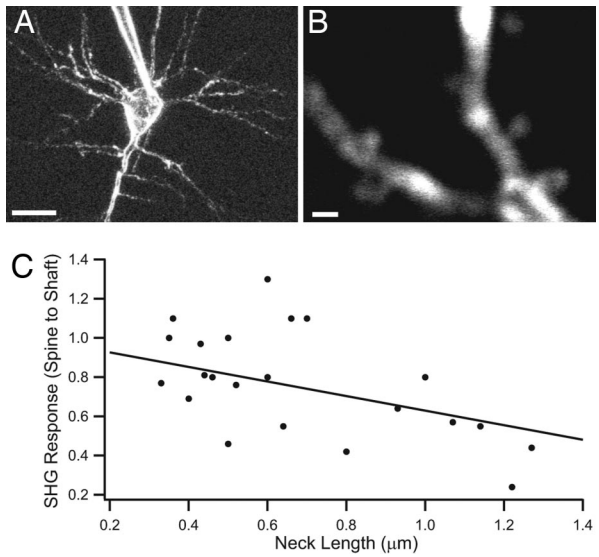

Fig. 5. Somatic voltage pulses are attenuated by the spine neck. (*A*) SHG image of a representative layer-5 pyramidal neuron, filled with FM 4-64, used for SHG spines voltage measurements. (*B*) High-resolution SHG image of dendritic spines on the basal dendrite. (*C*) Plot of normalized SHG response (SHG spine divided by SHG from adjacent dendritic shaft) vs. spine neck length. Line is the linear fit of the data, forcing the fit to cross the (0, 1) point. A similar fit was obtained without this requirement. For values, see *Results*. (Scale bars: *A*, 20 μm; *B*, 1 μm.)

Discussion

In this study, we inquired whether the spine neck filters membrane potentials, an idea proposed before (7–12) but not examined experimentally. We tested this idea by uncaging glutamate at spine heads while measuring the membrane potential responses at the soma and analyzed how those responses correlated with the neck length of the stimulated spines. We find that the longer the spine neck, the smaller the somatic potential. This correlation is strong and occurs independently of the location or size of the spine (Fig. 2*C* and Fig. 3). A similar correlation exists between the length of the spine neck and the rising kinetics of the uncaging potential, independently confirming the effect of the spine neck in filtering spine potentials (Fig. 3*A*). In the extreme case, we find a population of spines with very long necks that are electrically silent at the soma (Fig. 2). Those long spines have calcium transients comparable with those of short spines, as though the effect of the glutamate uncaging at their heads were similar (Fig. 4*B*). Finally, using SHG imaging, we find that long spines attenuate somatic voltages, as compared with shorter spines (Fig. 5). These results together reveal a strong effect of the spine neck in filtering membrane potentials.

We used glutamate uncaging at the head of the spine as a substitute of physiological synaptic input. Uncaging potentials were somewhat smaller and slower than spontaneous EPSPs, although larger uncaging potentials had similar risetime kinetics to spontaneous EPSPs. Differences in amplitude and kinetics are expected from the different spatiotemporal profile of the caged glutamate, released within a relatively large two-photon point spread function of our microscope (27), compared with the synaptic release of glutamate, precisely released in the synaptic cleft. Therefore, the spine neck could filter physiological EPSPs differently than uncaging potentials, so it is crucial to confirm whether the strong neck filtering we observe with uncaging potentials occurs also with physiological inputs. In fact, on the basis of the frequency dependency of cable filtering (12), we predict that the shorter physiological potentials might be filtered even more than the longer uncaging potentials. To test this prediction, an analysis of the correlation between the amplitude and kinetics of single-input EPSPs vs. the spine neck length could be performed for identified spines, activated physiologically (28). Another approach to determine the filtering of physiolog-

ical EPSPs could be using SHG imaging of membrane potential in spines heads and dendritic shafts in response to physiological EPSPs. Improvements in detecting spine SHG signals could make it possible to perform these measurements directly.

We did not encounter a relation between spine head diameter and uncaging potentials at the soma. This appears contrary to studies describing a linear correlation between spine volume and synaptic strength (29, 30), work performed in rat CA1 pyramidal neurons or rat olfactory cortex cultured cells. We cannot rule out that morphological analysis of the data with better spatial resolution could reveal such a correlation, once the neck effect is taken into account. At the same time, all our data were taken from mouse neocortical pyramidal neurons, so differences in results could be explained by area or species differences (19, 20).

On the basis of our results, we propose that the spine neck resistance is significant enough to attenuate synaptic potentials. Because the attenuation scales with neck length, and because a similar filtering is revealed in the slower rate of rise of uncaging potentials with increasing spine neck, this effect could be explained by passive cable properties of the neck length (12, 31). At the same time, given the prominence of active conductances in dendritic function (32, 33), their contributions are likely to be crucial. The engagement of even a few channels in the spine head or neck could profoundly alter the electrical structure of the spine. Further work is necessary to identify the distribution and functional properties of active conductances in spines.

Regardless of the exact mechanisms underlying the voltage attenuation by the spine neck, a direct implication of our data is that spines are electrical compartments and that the Vm at the spine head can differ from that of the parent dendrite, as demonstrated by our SHG measurements (Fig. 5). These data also indicate the difficulty in voltage-clamping long-necked spines. This electrical compartmentalization could enable local electrical events to occur at the spine, yet be invisible to the soma, consistent with Fig. 4. The electrical independence among spines could also explain why summation of inputs is linear on spines but sublinear on dendritic shafts (R.A., K.B.E., and R.Y., unpublished work). Also, given this electrical isolation, the presence of sodium channels at the spine head could enable the amplification of synaptic inputs (8, 12, 34) and of backpropagating action potentials (35) and even the generation of local action potentials at the spine head (10, 36, 37). In fact, our combined work indicates that sodium channels likely exist on spines, because we have previously documented full backpropagating action potential invasion into spines with SHG (17). Given the significant electrical filtering by the spine neck that we document now, we would argue that sodium channels must be present at the spine head to fully regenerate the action potential.

Finally, our findings have implications for the study of synaptic function and plasticity. Given the strong modulation that we observe to relatively slow signals because of the spine neck, it is likely that a similar, or even stronger, filtering could occur with physiological synaptic potentials. If this is indeed the case, changes in neck length would alter synaptic strength and form the morphological basis of synaptic plasticity, an idea proposed decades ago (9, 38). Moreover, because spine motility can quickly alter spine neck length (39), it could also quickly change synaptic strength. In addition, it is fascinating to consider the potential function of spines with long necks, which are more prominent in humans (19). We cannot rule out that, in response to a different stimulation protocol, the electrical contribution of these spines could be more prominent. Nevertheless, although these long-necked spines are activated by glutamate, we do not know at this time what their function could be. Long spines might represent silent synapses (40, 41) or perhaps be used as a reservoir of potential new functional connections during circuit rearrangements (42). Alternatively, long-necked spines could have a nonelectrical contribution to the cell biology of the postsynaptic neuron, perhaps as a storehouse of activated molecules that could diffuse to the dendritic compartment.

Materials and Methods

Slice Preparation. Animal handling and experimentation was done according to National Institutes of Health and local Institutional Animal Care and Use Committee guidelines. Mice were anesthetized with ketamine-xylazine (50 and 10 mg/kg^{-1}), and 300-μm thick coronal slices of visual cortex were prepared from P14-20 C57BL/6 mice as described (5).

Two-Photon Fluorescence Imaging and Electrophysiology. All experiments were performed at 37°C. Neurons were filled with 200 μM Alexa Fluor 488 (Molecular Probes, Eugene, OR) through the recording pipette. Pipette solution contained (in mM): 135 KMeSO4, 10 KCl, 5 NaCl, 10 Hepes, 2.5 Mg-ATP, and 0.3 GTP, pH 7.3. After cells were fully loaded with dye (15–30 min after break-in), dendritic location or spines were selected for imaging and uncaging. Imaging was done using a custom-made two-photon microscope (43), consisting of a modified Fluoview (Olympus, Melville, NY) confocal microscope and a Ti:Sapphire laser (Chameleon model; Coherent, Santa Clara, CA). A $\times$60, 1.1 N.A. objective (Olympus) was used to acquire images at the highest digital zoom ($\times$10). ImageJ (National Institutes of Health, Bethesda, MD; http://rsb.info.nih.gov/ij) was used to measure distances of the spines to the soma (site of the spine to location where parent dendrite emerged from the soma), spine head diameters (longest possible axis at any of frame in the z-stack of images), and neck lengths, measured from the proximal edge of the spine head to the edge of the dendrite or by computing the shortest orthogonal distance between the base of the spine head and the edge of the dendrite. This estimation was sometimes necessary because it was impossible to precisely ascertain the topology of the spine neck because of its small dimensions. For spines with no discernible necks, we chose a minimum value of 0.2 μm.

Two-Photon Uncaging of Glutamate. 4-methoxy-7-nitroindoline-caged L-glutamate (2.5 mM; Tocris Cookson, Bristol, U.K.) was bath-applied, and a Dynamax peristaltic pump (Rainin Instruments Inc., Woburn, MA) was used to control bath perfusion, recirculating the media and minimizing total bath volume. Imaging and uncaging were performed at 725 nm. The laser was positioned at $\approx$0.2 μm from spine heads of layer-5 pyramidal neurons that were filled with 200 μM Alexa Fluor 488 through recording pipettes. Laser power was controlled by a Pockels cell (Quantum Technology, Lake Mary, FL), gated with square voltage pulses (Master-8; AMPI, Jerusalem, Israel). For uncaging, 4-ms laser pulses at 2-s intervals were used with 25–30 mW of power on the sample plane. Uncaging potentials normally lasted $\approx$40–300 ms, much longer-lasting than the 4-ms uncaging pulses. For imaging, 5–8 mW of laser power was used. Voltage deflections due to the glutamate uncaging (uncaging potentials) were recorded from the soma in whole-cell current-clamp mode, maintaining a resting potential of $-$65 mV, by using Axoclamp 700B (Molecular Devices, Union City, CA) amplifier and analyzed offline. Physiological data were analyzed blind to the morphology of the spine. Data were analyzed with MATLAB (MathWorks, Natick, MA) and Igor (WaveMetrics, Inc., Lake Oswego, OR).

Calcium Measurements. Neurons were filled with 200 μM Calcium Green-1 (Molecular Probes) through the recording pipette. Pipette solution was otherwise the same as described above. About 30 min after break-in, spines were selected for imaging and uncaging. First, the laser was positioned at the spine head for 500 ms at a low imaging power level (Fig. 4*A*, Laser on spine head), then a 4-ms high-power, uncaging laser pulse (Fig. 4*A*,

Glutamate uncaging) was generated at the position indicated by a red dot in Fig. 4*B*, and this was immediately followed by repositioning the laser for 1 s at the same spine head location for calcium imaging again at low power levels. Calcium signals were collected with a photomultiplier tube (H7422P-40; Hamamatsu, Hamamatsu City, Japan). Averaged calcium signals from spine heads were calculated with 4-ms window smoothing and used to calculate the percentage change in basal fluorescence, expressed as $\Delta F/F$.

SHG Measurements. Measurements of membrane potential in spines and adjacent dendritic shafts were performed as described in ref. 17. Briefly, neurons were filled with 500 μM FM 4-64 dye (Biotium Inc., Hayward, CA) via the patch pipette. SHG imaging was started when cells were stained with the dye for 30–60 min after breaking in and performed on a different custom-made, two-photon laser scanning microscope (43) with a Nd:glass laser at 1,064 nm (IC-100, HighQ Laser). SHG signals were collected with a photomultiplier tube (Hamamatsu; H7422P-40) after a narrow band-pass filter (530/20). Slow somatic dc voltage pulses (30–50 mV in amplitude, 5–25 s in duration) were delivered by the patch pipette in voltage-clamp mode, while SHG intensity of dendritic shaft and spines was collected at a frame rate of 1–5 s per frame and averaged online. These voltage pulses were repeated 5–10 times to calculate the SHG changes of the dendritic shaft and spine head. Spines were selected on the basis of their signal to noise. There was no statistical correlation between the neck length and SHG baseline intensity ($R = 0.026$, $P = 0.91$), effectively ruling out potential artifacts because of systematic differences of chromophore diffusion into long spines.

Unless otherwise mentioned, data are reported as mean ± SEM and two-tailed Student's *t* tests were used.

We thank V. Nikolenko for help with the uncaging and C. Stevens and members of the laboratory for comments. This work was supported by the National Eye Institute, the Pew Programs in the Biomedical Sciences, and the New York STAR Center for High Resolution Imaging of Functional Neural Circuits. K.B.E. was supported by grants from the National Science Foundation.

1. Shepherd G (1996) *J Neurophysiol* 75:2197–2210.
2. Harris KM, Kater SB (1994) *Annu Rev Neurosci* 17:341–371.
3. Yuste R, Denk W (1995) *Nature* 375:682–684.
4. Denk W, Sugimori M, Llinás R (1995) *Proc Natl Acad Sci USA* 92:8279–8282.
5. Goldberg J, Tamas G, Aronov D, Yuste R (2003) *Neuron* 40:807–821.
6. Soler-Llavina GJ, Sabatini BL (2006) *Nat Neurosci* 9:798–806.
7. Chang HT (1952) *Cold Spring Harbor Symp Quant Biol* 17:189–202.
8. Llinás R, Hillman DE (1969) in *Neurobiology of Cerebellar Evolution and Development*, ed Llinas R (American Medical Association Education and Research Foundation, Chicago), pp 43–73.
9. Rall W (1970) in *Excitatory Mechanisms, Proc 5th International Meeting of Neurobiologists*, eds Andersen P, Jansen J (Universitets Forlaget, Oslo), pp 175–187.
10. Diamond J, Gray EG, Yasargil GM (1970) in *Excitatory Mechanisms, Proc 5th Internation Meeting of Neurobiologists*, eds Andersen P, Jansen J (Universitets Forlaget, Oslo), pp 213–222.
11. Rall W, Rinzel J (1973) *Biophys J* 13:648–688.
12. Jack JJB, Noble D, Tsien RW (1975) *Electric Current Flow in Excitable Cells* (Oxford Univ Press, London).
13. Tsay D, Yuste R (2004) *Trends Neurosci* 27:77–83.
14. Koch C, Zador A (1993) *J Neurosci* 13:413–422.
15. Svoboda K, Tank DW, Denk W (1996) *Science* 272:716–719.
16. Bloodgood BL, Sabatini BL (2005) *Science* 310:866–869.
17. Nuriya M, Jiang J, Nemet B, Eisenthal KB, Yuste R (2006) *Proc Natl Acad Sci USA* 103:786–790.
18. Matsuzaki M, Ellis-Davies GC, Nemoto T, Miyashita Y, Iino M, Kasai H (2001) *Nat Neurosci* 4:1086–1092.
19. Benavides-Piccione R, Ballesteros-Yañez I, DeFelipe J, Yuste R (2002) *J Neurocytol* 31:337–346.
20. Konur S, Rabinowitz D, Fenstermaker V, Yuste R (2003) *J Neurobiol* 56:95–112.
21. Ellis-Davies GCR (2003) *Methods Enzymol* 360A:226–238.
22. Eisenthal KB (1996) *Chem Rev* 96:1343–1360.
23. Millard AC, Lewis A, Loew L (2005) in *Imaging in Neuroscience and Development*, eds Yuste R, Konnerth A (Cold Spring Harbor Lab Press, Cold Spring Harbor, New York), pp 463–474.
24. Pons T, Moreaux L, Mongin O, Blanchard-Desce M, Mertz J (2003) *J Biomed Opt* 8:428–431.
25. Dombeck D, Blanchard-Desce M, Webb W (2004) *J Neurosci* 24:999–1003.
26. Nemet B, Nikolenko V, Yuste R (2004) *J Biomed Optics* 9:873–881.
27. Majewska A, Yiu G, Yuste R (2000) *Pflügers Arch Eur J Physiol* 441:398–409.
28. Markram H, Lubke J, Frotscher M, Roth A, Sakmann B (1997) *J Physiol (London)* 500:409–440.
29. Schikorski T, Stevens C (1999) *Proc Natl Acad Sci USA* 96:4107–4112.
30. Noguchi J, Matsuzaki M, Ellis-Davies GC, Kasai H (2005) *Neuron* 46:609–622.
31. Rall W, Rinzel J (1971) *Soc Neurosci Abstr* 1:64.
32. Johnston D, Magee JC, Colbert CM, Christie BR (1996) *Ann Rev Neurosci* 19:165–186.
33. Yuste R, Tank DW (1996) *Neuron* 16:701–716.
34. Johnston D, Wu SM-s (1995) *Foundations of Cellular Neurophysiology* (MIT Press, Cambridge, MA).
35. Tsay D, Yuste R (2002) *J Neurophysiol* 88:2834–2845.
36. Perkel DH (1982) *J Physiol (Paris)* 78:695–699.
37. Segev I, Rall W (1988) *J Neurophysiol* 60:499–523.
38. Rall W (1974) in *Studies in Neurophysiology*, ed Porter R (Cambridge Univ Press, Cambridge, UK), pp 203–209.
39. Majewska A, Tashiro A, Yuste R (2000) *J Neurosci* 20:8262–8268.
40. Isaac J, Nicoll R, Malenka R (1995) *Neuron* 15:427–434.
41. Liao D, Hessler N, Malinow R (1995) *Nature* 375:400–404.
42. Le Be J, Markram H (2006) *Proc Natl Acad Sci USA* 103:13214–13219.
43. Nikolenko V, Nemet B, Yuste R (2003) *Methods* 30:3–5.